ФИЗИКА ЭЛЕМЕНТАРНЫХ ЧАСТИЦ И АТОМНОГО ЯДРА
2005. Т. 36. ВЫП. 2

УДК [51-72:530.145]+[51-72:541.1]

MOLECULAR DYNAMICS SIMULATIONS OF RHODOPSIN AND PRION PROTEINS: THE EFFECT OF DISEASE-RELATED AMINO ACID MUTATIONS ON THE STRUCTURAL CONFORMATIONS

K. T. Kholmurodov

Joint Institute for Nuclear Research, Dubna

ФИЗИКА ЭЛЕМЕНТАРНЫХ ЧАСТИЦ И АТОМНОГО ЯДРА
2005. Т. 36. ВЫП. 2

УДК [51-72:530.145]+[51-72:541.1]

MOLECULAR DYNAMICS SIMULATIONS OF RHODOPSIN AND PRION PROTEINS: THE EFFECT OF DISEASE-RELATED AMINO ACID MUTATIONS ON THE STRUCTURAL CONFORMATIONS

K. T. Kholmurodov[*]

Joint Institute for Nuclear Research, Dubna

Molecular Dynamics (MD) simulations were performed to investigate the structural conformation of the rhodopsin and human prion proteins. We have estimated the effect of specific disease-related amino acid mutations on the dynamics and conformational changes. For the rhodopsin (Rh) protein we performed 3-ns simulations and presented the structure analysis data for the dark-adapted state of Rh. The RMSD (root-mean-square deviation) data for helices I–VII of Rh were evaluated. From the analysis of the RMSDs we observed a relative movement of Rh helices, which possesses not a similar behavior for all the helices. Helices I, III and V exhibit the highest deviations from the reference structure. The stucture images of Rh were constructed and the representative configurations were compared for the 3-ns state. The results show the largest displacements from the reference structure for helices III and V. The largest deviations are seen in the cytoplasmic region of these helices, the extracellular ends show slight movement. We have also simulated the effect of the E134N mutation on the Rh conformation dynamics. The E134N mutation has been considered to be important in the functionality of Rh. We have evaluated the RMSD behavior for the wild-type Rh protein and Rh with E134N mutation. The comparison of the analysis data indicated that the reference and E134N mutant structures are subjected to a similar behavior. The relative helical movement of the Rh protein seems to be sensitive mostly in the cytoplasmic region. The MD simulations were performed on three models of the human PrP (about 2 million time step/each structure) to investigate the effect of the specific disease-related point mutations on the conformation dynamics. We observed a partial rearrangement of the prion structure due to a $Glu^{200} \rightarrow Lys$ mutation, and provided a detailed mechanism of this process.

Молекулярно-динамическое (МД) моделирование выполнено с целью исследования структурных конформаций белков родопсина и преонов. Исследовано влияние замещения аминокислот, связанного с возникновением заболеваний, на динамику и конформационные изменения белков. Для белка родопсина (Rh) выполнены 3-нс МД-вычисления и представлены данные структурных анализов для «темного состояния» Rh. Значения RMSD (среднеквадратичные отклонения) оценены для отдельных структурных спиралей I–VII белка Rh. Анализ и сравнение вычислительных данных RMSD показывают внутримолекулярные относительные смещения спиралей

[*]The temporary research position where investigations are performed: Computational Astrophysics Laboratory, Advanced Computing Centre, RIKEN (The Institute of Physical and Chemical Research), Hirosawa 2-1, Wako, Saitama 351-0198, Japan.

Rh, которые не сходны друг с другом. Спирали I, III и V показывают наибольшие отклонения от исходных структур. Картинки (snapshots) структурных данных строились и сравнивались для исходной и конечной конфигураций. Результаты показывают наибольшие отклонения от исходных положений для спиралей III и V в структуре белка Rh. Эти наибольшие отклонения спиралей отчетливо прослеживаются в цитоплазмическом домене белка; внешняя (extracellular) часть Rh показывает относительно слабое смещение. Было также оценено влияние аминокислотного (мутационного) E134N-замещения на динамику конформационных изменений Rh. Вышеназванное E134N-замещение рассматривается с точки зрения экспериментального изучения как один из главных факторов в механизме функционирования белка Rh. Анализ полученных вычислительных данных и их сравнение указывают на сходность конформационных свойств нормального Rh и белка с E134N-замещением. МД-моделирование также проводилось над тремя моделями человеческого белка преона (human PrP). Оценено влияние болезнетворных мутантов (аминокислотных замещений), связанное с возникновением заболевания Крейцфельдта–Якоба, на динамику и конформационные изменения PrP. Обнаружено частичное разрушение структуры белка PrP как следствие аминокислотного $Glu^{200} \rightarrow Lys$-замещения, и представлен механизм данного процесса (структурной неустойчивости) на молекулярном уровне.

INTRODUCTION

The protein structural transformation issues (folding processes, conformational changes, mutation induced degenerations, etc.) are known to be the best targets for the molecular dynamics (MD) simulation technique [1–3]. The MD method allows one to describe the structural dynamics of biological systems (DNA and proteins) with a high accuracy. By the MD method one can efficiently compute the most probable states of DNA and proteins, to find their structural forms, to simulate the mutation transition processes and other related phenomena [4–6]. In the present study we have employed the MD simulation to investigate conformation dynamics of the rhodopsin and prion proteins. We have aimed to estimate the effect of the specific disease-related amino acid mutations on the structural conformation of the above proteins.

Retinal proteins (rhodopsins), a superfamily of the membrane receptors (known as GPCRs, G-protein-coupled-receptors), are involved in conversion of light to chemical energy and vision [7–9]. The outer layer of the retina segment comprises about 130 million photoreceptor cells (rods and cones), providing chromatic (color) images of high spatial resolution and achromatic vision with less spatial resolution [7, 10–12]. All rhodopsins contain the molecule retinal as their chromophore, and the activation of rhodopsins is initiated during a very short time (200 fs) through photo-induced isomerization events of the retinal chain around specific double bond [13–15]. Rhodopsin (Rh) is composed of seven transmembrane helical protein, opsin, and of retinal, a polyene chain bound to the protein through protonated Schiff base linkage to Lys^{296}. The mature form of the biomolecule Rh is comprised of 338 amino acid residues in total and its high-resolution crystal structure is available [7, 13]. Resonance Raman-spectroscopy experiments on Rh photoisomerization discovered that the light energy during

the absorption of photon energy and Rh photocycle is stored through a chromophore structural distortion. Time-resolved UV/VIS spectroscopy measurements have shown that Rh photocycle process involves several intermediates [15, 16]. Consequently, many recent computer molecular studies have been aimed to the theoretical description of the Rh isomerization and its conformational relaxation processes [17,19,20]. In [20], for example, MD simulations have been performed on Rh model embedded in the lipid bilayer and water environment. Retinal was isomerized around $C_{11} = C_{12}$ double bond, changing its conformation from 11-*cis* to all-*trans*, in accordance to the experimental observations [21–26]. However, the nature of nonreaction dynamics and conformation of the Rh is still unknown. It is also worth noting that dynamics of retinal photoisomerization is strongly influenced by its environment (opsin + solvent) [15, 18].

In today's molecular modeling the Rh conformation and its photo-induced isomerization are mostly studied by the conventional and quantum-mechanical molecular dynamics (MD and ab initio QM/MM) methods [11, 17–20]. It is worth noting that although the ab initio QM provides for a basic insight into the reaction mechanism, the actual dynamics paths can deviate from the MEP (this is due to thermal fluctuations, reaction excess energies, etc.). For example, the characteristic of the incoherent kinetics and dynamics can be directly captured through the only MD simulations [20]. The above facts just emphasize the importance of MD simulations in computational studies of Rh.

In the present work we investigated the Rh conformation dynamics in the dark-adapted state. We were aimed to estimate the induced effect of the specific, disease-related amino acid point mutations (for example, E134N and others [11, 13, 15]) on the Rh conformation. The 3-ns MD simulations were performed on Rh to study its conformation behavior in an explicit (water) solvent [27]. We have also compared the effects of the cutoff and no cutoff approximations [27,28] on the protein final (2.0 ns) configuration. To elucidate these we have examined: 1) the dynamics of the structural conformations of Rh; 2) correlations between the cutoff and no cutoff molecular interactions and structural changes of Rh. The root-mean-square deviations (RMSD) have shown that the RMSD of the Rh model for no cutoff method was kept at around 0.7 Å for the 500 ps simulation, which indicates the structural stabilities of the model. The RMSD of the cutoff method is comparably two times larger than that of no cutoff simulations. It gradually increased to from the same point of around 0.7 Å, at the start of simulation, and then it increases within a short time 20–60 ps. The RMSD for the cutoff simulations finally fluctuates in the region of 1.3–1.5 Å after about 200 ps. Thus, in the cutoff method the Rh protein seems undergoes essential conformational changes, when the RMSD is considerably increased.

The structural and functional properties are known often to correlate well for a number of proteins. This fact can be observed more obviously, for example, for the prion proteins [29–32]. It is well understood that the misshapen prion

protein (today cell biology challenging topic) is generally associates with its disease-related form [33, 34]. In the normal human prion protein (PrP) the prion molecules are coiled into helix and help to maintain the integrity of the nerve cells. As theoretical and experimental observations show, the infectious prion proteins are more sheet-like and coax normal prions to fold into infectious (disease-related) form [33, 35]. Thus, a central question of the physiological functionality of the normal prion protein (PrP^C) and its aberrant form (PrP^{Sc}) has to be closely connected with their structural transformations.

In [36–38] we have performed MD simulations on the human PrP to elucidate the effect of point mutations related to the inherited Creutzfeldt–Jakob disease (CJD) [29, 35]. We examined and compared the structural changes of the human PrP through the consideration of three NMR structures (the wild-type prion and two mutant structures with $Glu^{200} \to Asp$ and $Glu^{200} \to Lys$ substitutions). In this study we present the analysis of the dihedral angles and residue distance distributions in detail.

1. SIMULATION ASPECTS OF THE INFLUENCE OF SPACE FORM RADIATIONS ON VISION SYSTEM: THE STRUCTURAL TRANSFORMATIONS OF RETINAL PROTEINS (RHODOPSINS) AND THEIR ISOMERIZATION INTERMEDIATES

There is a problem of great importance for the nearest future how to realize long-time missions in space, to the outer magnetosphere (Mars project) [39]. The most difficulties of this issue are related with the existence in Galactic space of a wide range of radiation spectrum (in charge and energy), caused by the effect of the heavy charged particles. One of the most critical (sensitive) systems to such a kind of influences is a vision complex of the eye, first of all the retina and lens [7, 12, 40, 41]. The Joint Institute for Nuclear Research (JINR) has an excellent possibility to simulate the influence of the space form radiations on the vision complex (for example, with use of a new accelerator — Nuclotron). There have been collected a lot of the experimental data, regarding the effect of heavy charged particles on the eye system, which discover the following nontrivial phenomena [41–43]:

1) the irreversible changes of the retinal proteins (rhodopsins), presented in the outer segment of the rod cells, and of the retina as a whole (electroretinogram), which cannot be observed during the influence of the beams of electromagnet nature;

2) the essential structural changes in the crystallines, the proteins which form the lens basic functions, caused by the heavy particles irradiation.

The influence of heavy charged particles (e.g., deuterons) on the isolated frog retina:

• the effect of heavy charged particles induces ERG (electroretinogram) and LRP (late receptor potential), that are similar to the light-induced ERG and LRP;

• however, in contrast to light irradiation, the deuteron irradiation leads to the irreversible disappearance of the retina's electrical activity.

For the visual pigment, Rhodopsin (Rh), the experimental studies observe the following phenomena [39, 41]:

• the deuterons irradiation leads to a bleaching of Rh — the absorption spectra of the final products are indistinguishable from the known spectra of the final products of the Rh photolysis;

• however, as a result of deuterons irradiation, the Rh molecule is damaged — the loss of ability to regenerate after adding the 11-*cis* retinal to the deuteron-irradiated Rh.

The understanding of mechanisms of the structural and functional changes, which occur in the irradiated eye tissues, will inevitably involve the use of the computer simulations (for example, the MD method) [1, 2, 5, 44–49]. The MD simulation, one hopes, can provide a possibility of numerical analysis of the experimental results and to estimate the rate of nondesirable risks. From the point of view of rather a broad statement as well as from the long-term perspectives (in supporting of the experimental data analysis) our objectives on the use of the MD simulations could be outlined as follows:

• conformational changes of the rhodopsin in the dark-adapted states (with the free retinal, Rh + 11-*cis* retinal, Rh + 9-*cis* retinal, Rh + 13-*cis* retinal, etc.);

• primary photoinduced activation of the rhodopsin proteins and their isomerization events (intermediates with Rh + 11-*cis* retinal, etc.);

• the mechanisms of the structural and functional changes, which occur in the irradiated eye tissues (site-directed mutagenesis of Rh, stochastic effects of the radiation-induced mutations, etc.).

In the sections followed we demonstrate the effects of the computer MD simulations on conformational dynamics of Rh proteins in the solvent (water) environment.

2. THE PRIMARY PHOTO-INDUCED ISOMERIZATION OF RHODOPSIN

The analysis of the electron density data on the 11-*cis*-retinal chromophore and transmembrane helices [7, 13] provides some preliminarily picture of the intermolecular interactions in the Rh protein. In Fig. 1 the Rh ribbon structure with a retinal chromophore are presented. From the intradiscal side of the Rh the retinal chromophore has positioned in a way that it equally separates the protein into the cytoplasmic and extracellular regions. The structural conformation of the retinal chromophore in Rh has to be stabilized by a number of the interhelical

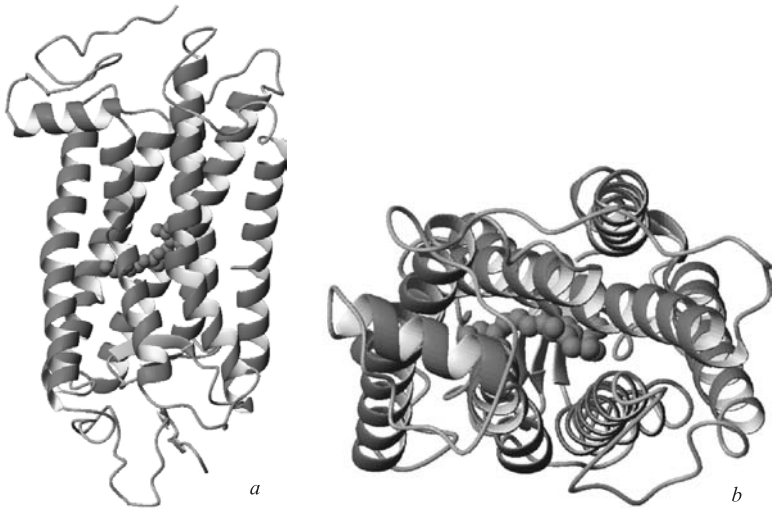

Fig. 1. The Rh ribbon structure and chromophore at the initial state: *a*) view from the extracellular side; *b*) view from the cytoplasmic side. The retinal polyene chain is drawn as balls

hydrogen bonds and hydrophobic interactions (dominantly by helices I–V of the Rh). Most of the interhelical interactions (in helices I–V) are mediated by highly conserved residues in G-protein coupled receptors (GPCRs) [13, 50–52]. A binding pocket environment of the 11-*cis*-retinal chromophore from the Rh cytoplasmic part are the important intermolecular side chains, surrounding the 11-*cis*-retinylidene group [7, 13, 51].

The structural conformations of the Rh essentially determine its function as a light-activated receptor. In the dark state we have a Rh + 11-*cis* retinal configuration. Photoinduced isomerization of the chromophore results in Rh + all-*trans* retinal state [8, 15]. In the dark state the (11-*cis*) retinal stabilizes the inactive conformation of Rh. Its isomerization (all-*trans*) triggers Rh transition to an active state, which catalyzes the GDP/GTP exchange. Thus, the chromophore conformational change from the 11-*cis* to all-*trans* triggers a transition of the Rh receptor to the active state, initiating the exchange of the GDP for GTP in α-subunit of the transducin, a G protein associated with Rh [13, 20].

It is worth noting that the rhodopsin (Rh), bacteriorhodopsin (bR) and halobacteria rhodopsin (hR) are members of the transmembrane proteins family, that emerge similar conformational properties [10]. They possess, for example:

- the same number of transmembrane helices;

• the topography of the polypeptide chain arrangement across the lipid bilayer;

• the position of the lysine side chain to which retinal is attached.

The structure and functions of Rh and bR (hR), however, are completely different from each other. For example, the bR conformation (as a light-driven proton pump) in the light-adapted state is a bR + all-*trans* retinal [13, 50–52]. Through the bR photoisomerization process we have a bR + 13-*cis* retinal state, which is a structurally different configuration in comparison with the Rh as described above. Also, the bR transition from all-*trans* to 13-*cis* configuration triggers a photocycle process in which one proton is pumped from the cytoplasmic side to the extracellular part of the membrane [7, 53, 54].

In Fig. 2, *a* a molecular structure diagram of a retinal chromophore is presented. Figure 2, *b* displays a retinal polyene chain with six double bonds, bounded to Lys^{216} (Lys^{296} for Rh) via a Schiff base. As the resonance Raman-spectroscopy experiments have shown, the light energy in Rh is stored through structural distortion of the retinal chromophore [7, 15]. The activation of the Rh is initiated, as was noted above, by a retinal photoisomerization around a specific double bond ($C_{11} = C_{12}$ in Rh, $C_{12} = C_{13}$ in bR, etc). The Rh photocycle process involves several intermediates [15], which are detected experimentally at the cryogenic and room temperatures (PHOTO-Rh (570 nm absorption specra, within 150 ns), BATHO-to-BSI (529 nm absorption specra and 5 ps), LUMI (μs), META-I (ms) and META-II). The retinal binding pocket has to be large

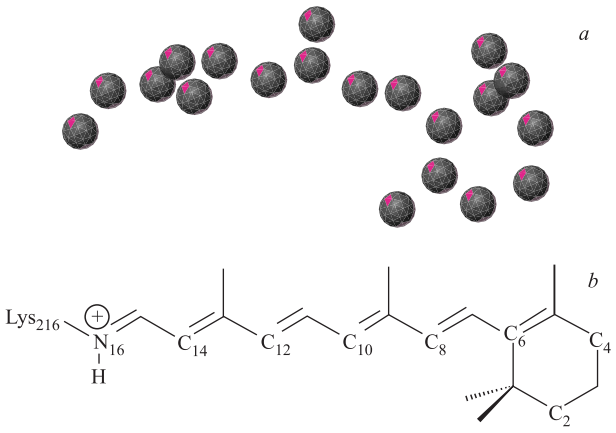

Fig. 2. A molecular structure (*a*) and a schematic diagram (*b*) of the retinal chromophore are drawn. The positions of the beta-ionone (right) ring and Schiff base linkage (left) are shown

and enough flexible to accomodate a variety of chromophores [13, 20]. Its large motion is accompanied, for example, with BATHO-to-BSI transition or implies the rotation of the helix IV [14, 16]. Thus, the retinal binding sites or salt bridges in the Rh are evidently correlate with the activation mechanism of the protein. For example, the Rh activation is associated with a shift of the relative orientation of helices III and VI [11, 20]. The Schiff group and Glu^{113} binding stabilize the connection between helices III and VII, the disruption of this binding site activates Rh at the absence of the retinal chromophore. In later photoisomerization stages (META-I and META-II intermediates) the major conformational changes of the Rh have to occur. Finally, in META-II the Schiff base proton has to transfer to the Glu^{113} amino acid [15, 55, 56].

3. MD SIMULATIONS ON THE RHODOPSIN STRUCTURAL CONFORMATIONS

The correlation of Rh conformational dynamics and its activation process at later stages are the most challenging targets in computer molecular simulations of Rh. The relative movement of the Rh helices could be a part of a Rh light-activated photocycle [11]. The expriments revealed that a movement of Rh helices (for example, a movement of helix VI relative to other helices) plays a key role in Rh activation [57, 58]. This evidently motivates the extremely time consuming atomic modelling of Rh. It has been considered that the large-scale motion of Rh may be a common dynamic motion for other alpha-helical G-protein receptors [11, 59].

We simulated the bovine Rh to study its conformation dynamics in the dark-adapted state. The molecular mechanics (MM) and MD simulations on Rh were performed with an explicit (water) solvent. A molecular model was constructed from the Rh crystal structure (PDB: 1HZX) [13, 14]. The missing amino acids 236–240 and 331–333 were inserted using the MOE software package for bio-molecular simulations [60]. Two sets of MD simulations (viz., cutoff and no cutoff calculations) were performed with the software package AMBER [5, 61]. We have used the program package AMBER 5.0 (Parm94, cutoff method) [61] on a supercomputer Fujitsu VPP and modified version of AMBER 7.0 (Parm96, no cutoff method) for a special-purpose computer MDGRAPE-2 [62–64]. The all-atom force field of Cornell et al. [65] was used in MD simulations. A system was solvated with TIP3P molecules [66] generated in a spherical (nonperiodic) water bath. The temperature was kept constant by using Berendsen algorithm with a coupling time of 0.2 ps [67]. Only bond lengths involving hydrogen atoms were constrained using the SHAKE method [68]. The cutoff distance of nonbonded interactions was 14 Å; for the MDGRAPE-2 all interactions were calculated. The integration time step in the MD simulations was 1 fs. The simulation procedures

were the same in all calculations. Firstly, a potential energy minimization was performed on an initial state for each system. Next, the MD simulation was performed on the energy-minimized states. The temperatures of the considered systems were gradually increased by heating to 300 K for and then kept at 300 K for the next 3 million time steps. The trajectories at 300 K for 3.0 ns were compared and studied in detail. The result of simulations and images of simulated proteins were analyzed by using the RasMol [69] and MOLMOL [70] packages.

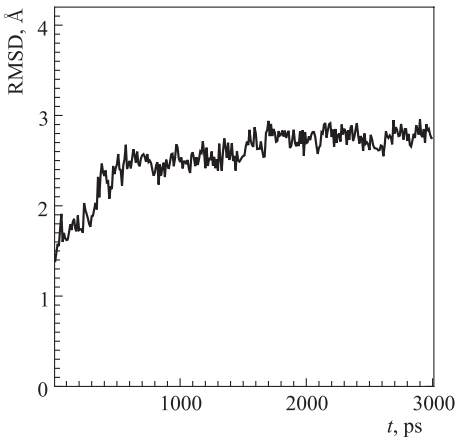

Fig. 3. The RMSD (root-mean-square displacement) for the Rh total structure domain within 3-ns state

Figure 3 shows the root-mean-square deviation (RMSD) for a total structure domain of the Rh protein. In Fig. 4 the separately calculated RMSD values for each of helices I–VII are presented. The RMSD values were evaluated for only the backbone atoms of the helices. The RMSD of the total Rh structure, as is seen from Fig. 3, has kept around 4.5 Å, which indicates a stability of the Rh structure during the 3.0-ns period of simulations. With regard to a selected Rh helix (Fig. 4) we observe a relative movement of Rh helices; displacements of Rh helices have not a similar behavior. Helices I, III and V exhibit the highest deviations from the reference structure.

In Fig. 5, *a* the superposition of the representative structures is presented at 3-ns state. Figure 5, *b* shows the largest displacements from the reference structure for helices III and V. The largest differences are seen in the cytoplasmic region of the helices; the extracellular ends show slight movement. Some reported MD studies indicate, for example, the largest RMSDs for helices I, V, and VI or helices IV, V, and VI [11, 57, 58]. It is worth noting that spin-label experiments show the movement of the cytoplasmic part for helices II, VI, and VII [20, 59].

Next we have simulated the effect of the E134N mutation on the Rh conformation dynamics. The Glu134Asn mutation has regarded to be an important site from the point of view of Rh protonation mechanism. For example, this mutation can activate transudin in the absence of the 11-*cis* retinal [15, 73]. In Fig. 6 the RMSD evolutions for the normal Rh and with E134N mutation are shown. In Fig. 7 the RMSD values for each of helices I–VII for both normal and mutant E134N Rh are presented. The comparison of the above pictures indicates that the reference and E134N mutant structures have generally a similar behavior. It is

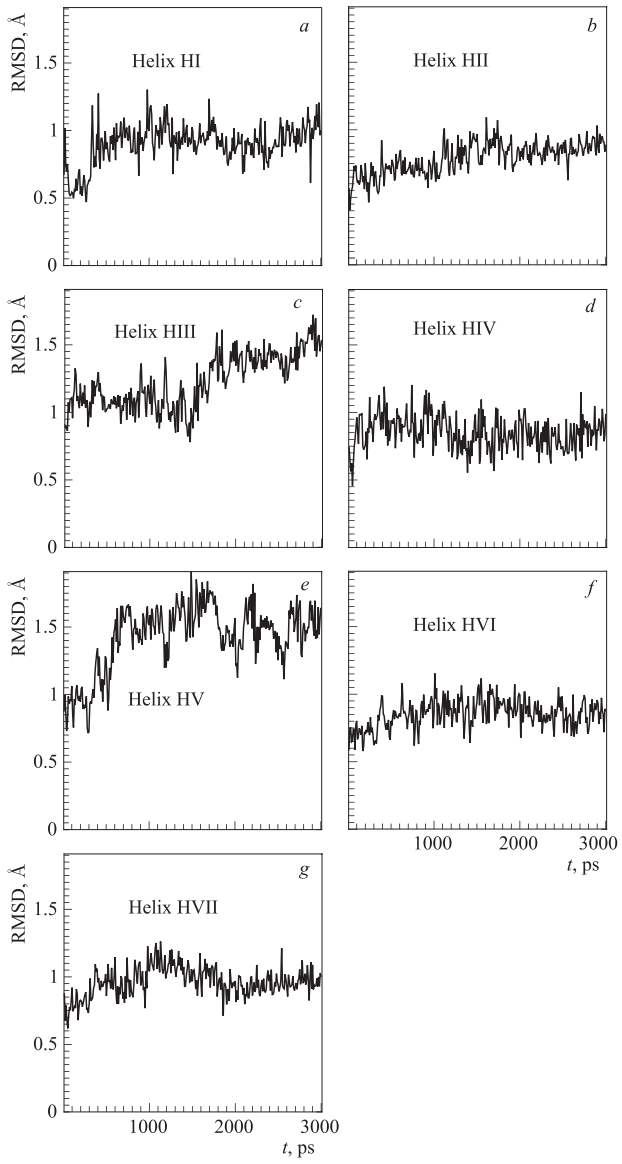

Fig. 4. The RMSDs for the helices I–VII of Rh are shown. The relative movement of the helices results in a nonlinear behavior between the RMSDs. The largest deviations are seen for helices I, III, and V

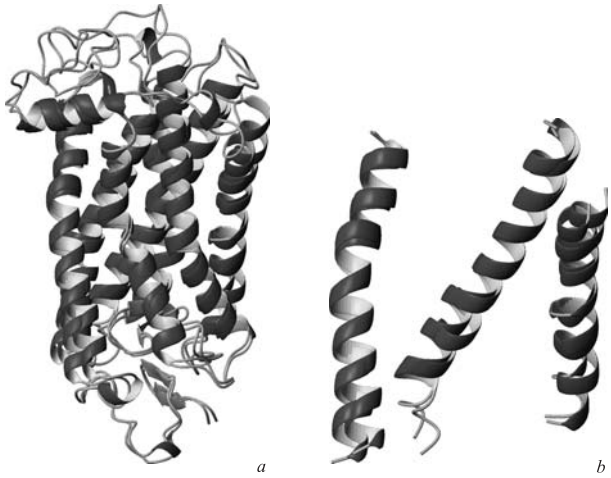

Fig. 5. *a*) The Rh ribbon structure at the initial and final (3 ns) states. *b*) The largest distortions are observed for helices I (left), III (middle) and V (right)

worth noting that nearly every residue in Rh has been examined with site-directed mutagenesis [58, 59, 71]. There have been several important amino acids (E134N, E122Q, D83N, etc.) to play an essential role in the Rh protonation mechanism mentioned above [72, 73]. Although, some molecular simulation results have been reported (see, for example, [11]), which suggest that the nature of dynamical transitions in Rh dark-adapted state has been governed by its collective motion and no single amino acid or particular defined sequence has been considered to be dominant. However, a great number of the experimental evidence ([13, 15, 21], etc.) reveal that a selected amino acid mutation may cause essential changes in the formation of Rh intermolecular interactions, mostly electrostatics. The presented simulation results support in general this statement.

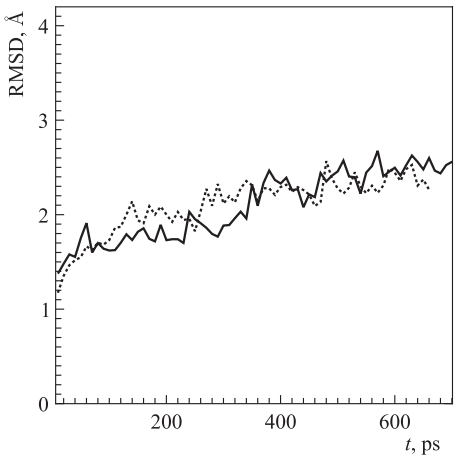

Fig. 6. The RMSD for the reference structure (solid line) and Rh with E134N exchange (dotted line) within 1-ns state are shown

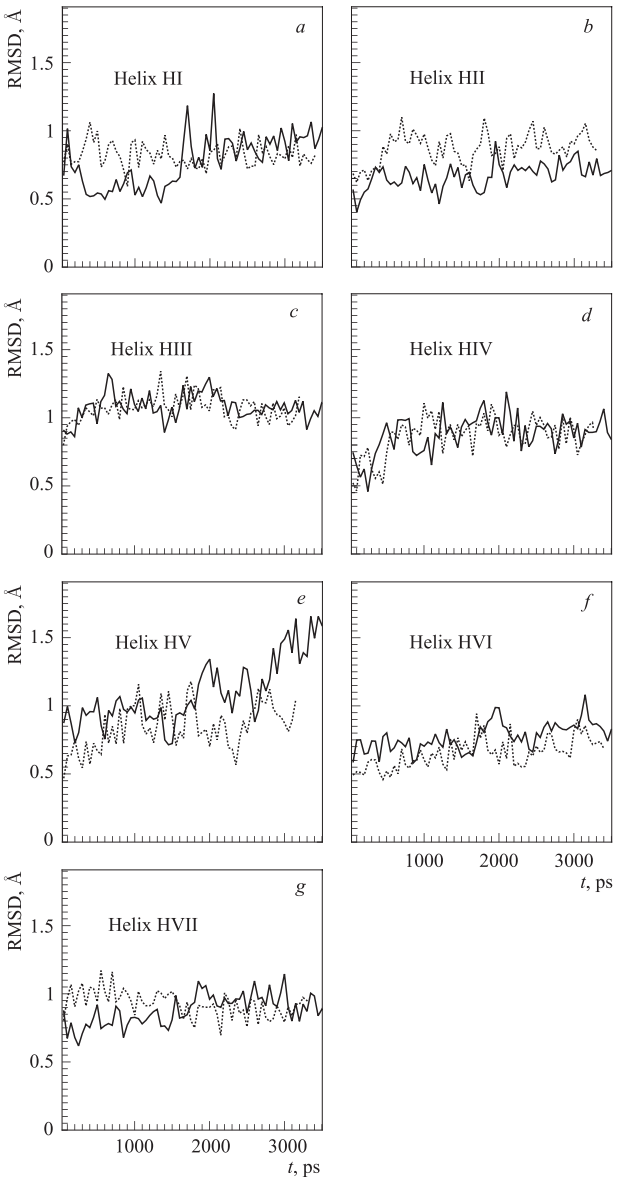

Fig. 7. The RMSDs for helices I–VII are shown for the reference structure (solid line) and Rh with E134N exchange (dotted line) within 1-ns state

4. THE CORRELATION OF THE STRUCTURE AND FUNCTIONS OF PRION PROTEINS

The prion protein (PrP) is a challenging topic of the cell molecular biology [74–76]. Prions are associated with an unusual class of neurodegenerative diseases, such as BSE (bovine spongiform encephalopathy) in cattle, include scrapie in sheep, and CJD (Creutzfeldt–Jakob disease), Gerstmann–Sträussler–Scheinker syndrome (GSS), fatal familial insomnia (FFI) in humans [29, 77–79]. The prion disease is caused by an abnormal form of the PrP, which accumulates in the plaques in the brain. New variant of CJD (nv-CJD) is a human form of the mad cow disease. The illness arises through eating beef tainted by the substance that causes mad cow disease, or BSE [80–82].

The prion diseases and other transmissible encephalopathies (TSEs) are characterized by the transformation of a normal prion protein (PrP^{C}) into an abnormal disease-related form (PrP^{Sc}) [29, 30, 77]. The function of prion proteins (of normal PrP^{C} or abnormal PrP^{Sc} form) is still unkown and this issue causes very tough studies, involving world-wide research investigations [75]. In the normal human PrP the prion molecules are coiled into helix and help to maintain the integrity of the nerve cells. The infectious prion proteins are more sheet-like and coax normal prions to fold into infectious (disease-related) form [83–87]. The disease-associated form PrP^{Sc} differs from its normal cellular form PrP^{C} only in three-dimensional structure; it has a significantly increased content of β-sheet conformation compared with PrP^{C}. For example, the experiments using circulator dichroism (CD) and Fourier-transform infrared (FTIR) analyses have shown that PrP^{C} has a low β-sheet content ($\approx 3\%$) and is sensitive to proteases, whereas PrP^{Sc} has a high β-sheet content ($\approx 30\%$) and is protease-resistant [16, 32, 79]. Thus, the physiological functionality of the normal PrP^{C} and its aberrant form PrP^{Sc} has closely been connected with their structural transformations.

The familial forms of prion diseases (for example, GSS, FFI, and CJD) are known to segregate with the exchange of individual amino acids or point mutations in the prion protein sequence [29, 34, 35, 80]. Point mutations in the human gene of PrP^{C} were seen in 102, 105, 117, 145, 198, 217 in GSS and 178, 200, and 210 in the most cases of CJD [30, 77, 89]. The mutation point 200, for example, caused a particular interest, this amino-acid residue has been associated with a famous type of the genetically transmitted CJD [88, 89]. We examined the correlation between the mutations at residue 200 and the protein structures. In [36–38] we have performed MD simulations on the human PrP to elucidate the effects of point mutations related to the inherited form of the CJD [29, 35]. We investigated and compared the structural changes of the human PrP through the consideration of three NMR structures (the wild type prion and two mutant structures with $\mathrm{Glu}^{200} \rightarrow$ Asp and $\mathrm{Glu}^{200} \rightarrow$ Lys substitutions). In the next sections we present the analysis of the dihedral angles and residue distance distributions for the above PrP models in detail.

5. MD SIMULATIONS ON THE DYNAMICS AND CONFORMATIONAL CHANGES OF PRION PROTEINS

The mature form of the human PrP comprises 208 residues (Fig. 8, numbered (23–230)) [86,90–92]. The C-terminal part of the polypeptide chain with residues 125–228 forms a compact globular domain and is stable, whereas the N-terminal part (21–124) is unstructured in aqueous solution at pH5 [93–95]. The C-terminal region containing domain (125–228) is shown by Fig. 9 (*a* — ribbon structure; *b* — schematic diagram of the globular domain with helices H1, H2, and H3).

														125	126	127	128	129	130
														L	G	G	Y	M	L
													—				*B*	*B*	*B*
131	132	133	134	135	136	137	138	139	140	141	142	143	144	145	146	147	148	149	150
G	S	A	M	S	R	P	I	I	H	F	G	S	D	Y	E	D	R	Y	Y
													A	*A*	*A*	*A*	*A*	*A*	*A*
151	152	153	154	155	156	157	158	159	160	161	162	163	164	165	166	167	168	169	170
R	E	N	M	H	R	Y	P	N	Q	V	Y	Y	R	P	M	D	E	Y	S
A	*A*	*A*	*A*							*B*	*B*	*B*	*B*						
171	172	173	174	175	176	177	178	179	180	181	182	183	184	185	186	187	188	189	190
N	Q	N	N	F	V	H	D	C*	V	N	I	T	I	K	Q	H	T	V	T
		A	*A*	*A*	*A*	*A*	*A*	*A*	*A*	*A*	*A*	*A*	*A*	*A*	*A*	*A*	*A*	*A*	*A*
191	192	193	194	195	196	197	198	199	200	201	202	203	204	205	206	207	208	209	210
T	T	T	K	G	E	N	F	T	E	T	D	V	K	M	M	E	R	V	V
A	*A*	*A*	*A*						*A*	*A*	*A*	*A*	*A*	*A*	*A*	*A*	*A*	*A*	*A*
211	212	213	214	215	216	217	218	219	220	221	222	223	224	225	226	227	228		
E	Q	M	C*	I	T	Q	Y	E	R	E	S	Q	A	Y	Y	Q	R		
A	*A*	*A*	*A*	*A*	*A*	*A*	*A*	*A*	*A*	*A*	*A*	*A*	*A*	*A*	*A*	*A*	*A*		

Fig. 8. A diagram of primary structure sequences of the human PrP

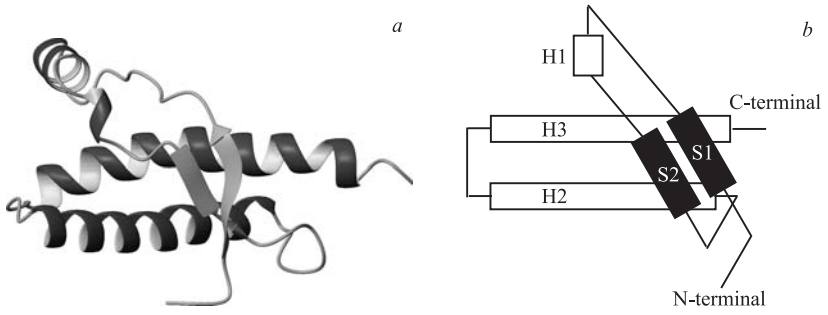

Fig. 9. A ribbon structure (*a*) and a schematic diagram (*b*) of globular domain of the human PrP. The structure consists of three α helices (H1, H2, and H3) and a short β sheet (S1 and S2)

We have performed MD simulations on three model structures of the human PrP. Model 1 is derived from the NMR structures of the human PrP (PDB code: 1QM2 [96]). The model includes a prion globular domain (a structured part, residues (125-228)), and we called model 1 «wild-type structure». Models 2 and 3 represent mutant structures containing $Glu^{200} \rightarrow Asp$ and $Glu^{200} \rightarrow Lys$ substitutions. These two models are built from the same NMR structure as for model 1. $Glu^{200} \rightarrow Lys$ in model 3 is a disease-related amino acid exchange, so we call this model an «abnormal-type structure». The wild-type PrP has a glutamate at 200 codon, the $Glu^{200} \rightarrow Asp$ and $Glu^{200} \rightarrow Lys$ substitutions occur just before the third helix (a longer, middle helix in Fig. 9). We have used the program package AMBER 5.0 [61] to perform the MM potential energy minimizations and MD simulations. The nonbonded interactions were calculated using the cutoff method ($r_{\mathrm{cut}} = 14$ Å). The details of simulations were the same as described in Sec. 2.

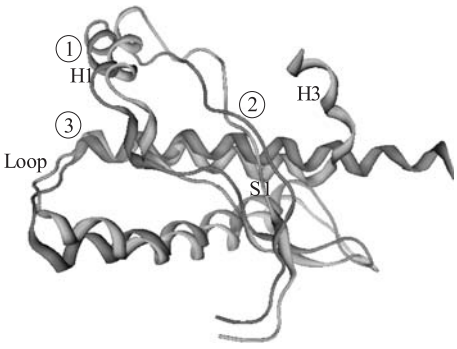

Fig. 10. The structure plots of the human PrP in model 3 (mutant $Glu^{200} \rightarrow Lys$ prion protein) for the initial and final states (1.6 ns)

Figure 10 shows the calculated structures for model 3 (mutant $Glu^{200} \rightarrow Lys$ prion protein) at the initial and final states. As is seen from Fig. 10, the structure of the mutant $Glu^{200} \rightarrow Lys$ prion has partly rearranged; we observe a collapse of the third (longest) α-helix H3. A structure destruction position is on the residue 219, where H3 rearranges to interact with the strand between H1 and S1. For the wild-type prion, as an analysis shows (the data are not shown), the globular domain stably maintains during the whole simulation period. A comparison of the pictures for the wild and abnormal $Glu^{200} \rightarrow Lys$-type prions suggests a mechanism of the structural reorganization as decribed above. Namely, when a glutamate to lysine substitution occurs (at the mutation point 200) the H1 and H3 come very close to each other. A flexible motion of H1 to H3 seems to result in the protein structural rearrangement. At the same time H3 interacts with the strand between H1 and S1 and forms probably a new hydrogen bond. As regards for model 2 (mutant $Glu^{200} \rightarrow Asp$ prion), its initial structural changes look almost the same as for the model 3. The longest α-helix H3 begins to bend at residue 219, in the same way as in model 3. However, the structure will not collapse completely, its final behavior is not like as that in Fig. 4, so the protein to be refolded properly.

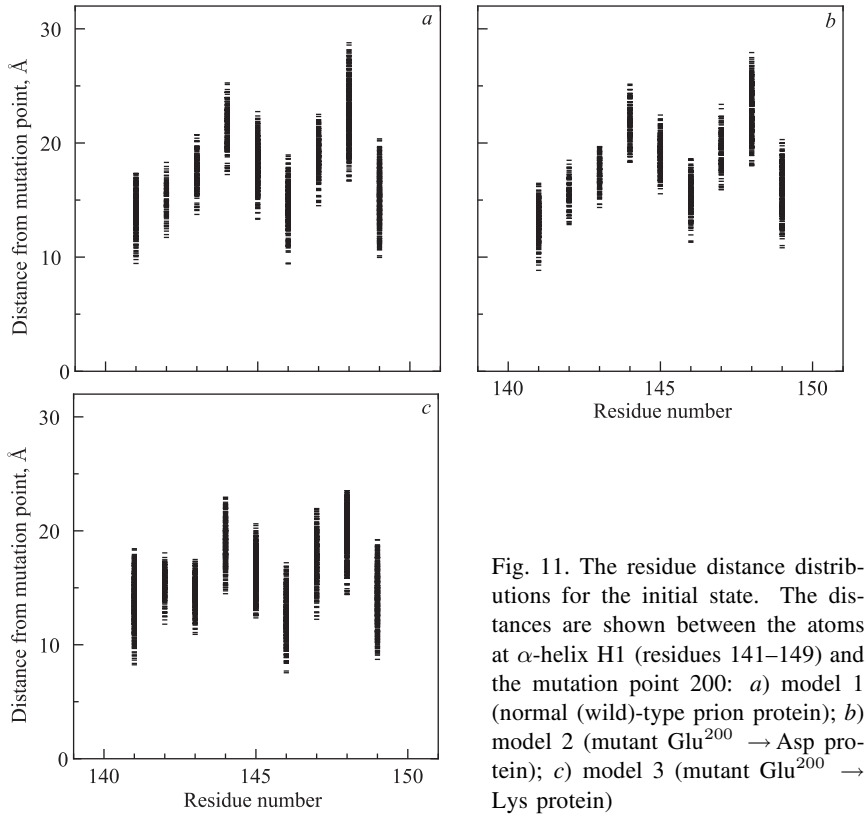

Fig. 11. The residue distance distributions for the initial state. The distances are shown between the atoms at α-helix H1 (residues 141–149) and the mutation point 200: *a*) model 1 (normal (wild)-type prion protein); *b*) model 2 (mutant $Glu^{200} \rightarrow$ Asp protein); *c*) model 3 (mutant $Glu^{200} \rightarrow$ Lys protein)

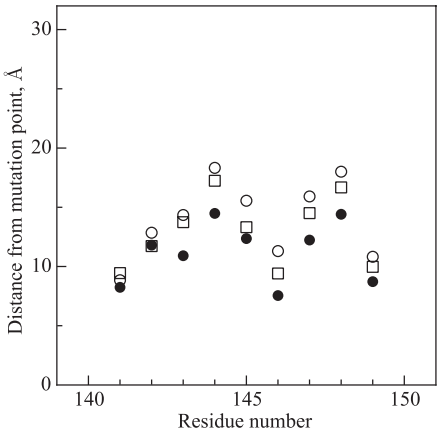

Fig. 12. The minimum residue distance distributions for the initial state. The minimum distances are shown between the atoms at α-helix H1 (residues 141–149) and the mutation point 200: □ — model 1 (normal (wild)-type prion protein); ○ — model 2 (mutant $Glu^{200} \rightarrow$ Asp protein); ● — model 3 (mutant $Glu^{200} \rightarrow$ Lys protein)

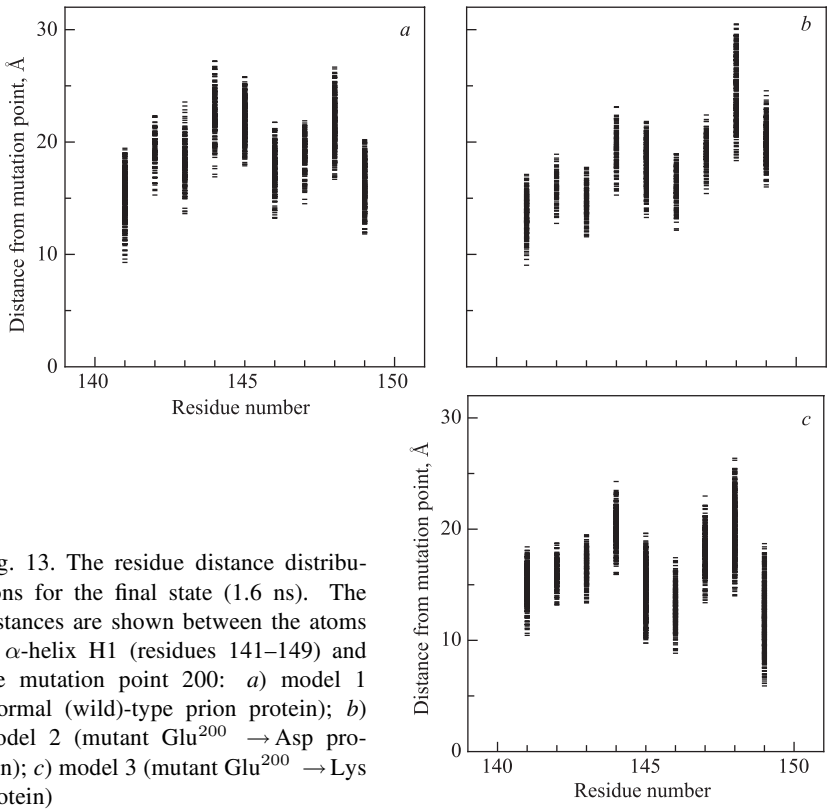

Fig. 13. The residue distance distributions for the final state (1.6 ns). The distances are shown between the atoms at α-helix H1 (residues 141–149) and the mutation point 200: *a*) model 1 (normal (wild)-type prion protein); *b*) model 2 (mutant $Glu^{200} \rightarrow$ Asp protein); *c*) model 3 (mutant $Glu^{200} \rightarrow$ Lys protein)

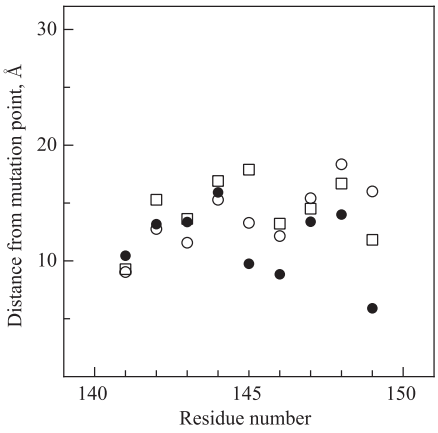

Fig. 14. The minimum residue distance distributions for the final state (1.6 ns). The minimum distances are shown between the atoms at α-helix H1 (residues 141–149) and the mutation point 200: □ — model 1 (normal (wild)-type prion protein); ○ — model 2 (mutant $Glu^{200} \rightarrow$ Asp protein); ● — model 3 (mutant $Glu^{200} \rightarrow$ Lys protein)

The analysis of the prion structures indicates that flexibility of the short α-helix H1 is very sensitive depending on the type of amino-acid substitution at the residue point 200. For the $Glu^{200} \rightarrow Lys$ mutation all the atomic positions of H1 look to be very close to the α-helix H3 (in contrast with other two protein models under consideration). We estimated the residue distance distributions of the α-helix H1 in detail. The H1 consists of 9 residues (numbered 141–149), for all of them we have calculated the atomic distance distributions to the mutation point 200. Figures 11 and 13 display the calculated distances between all the atoms of the residues at H1 and that of the residue 200 for the initial and final (1.6 ns) states, respectively (*a* — model 1; *b* — model 2; *c* — model 3). Figures 12 and 14 show the minimum distance distributions between the atoms of H1 and residue 200 (for the same states as in Figs. 11 and 13). It is clear that all three models at the begining of MD simulations have a similar atomic distance distribution. However, the more simulation proceeds the more distance distributions differ one from another. The residue distance distributions of models 1 and 2 look similar.

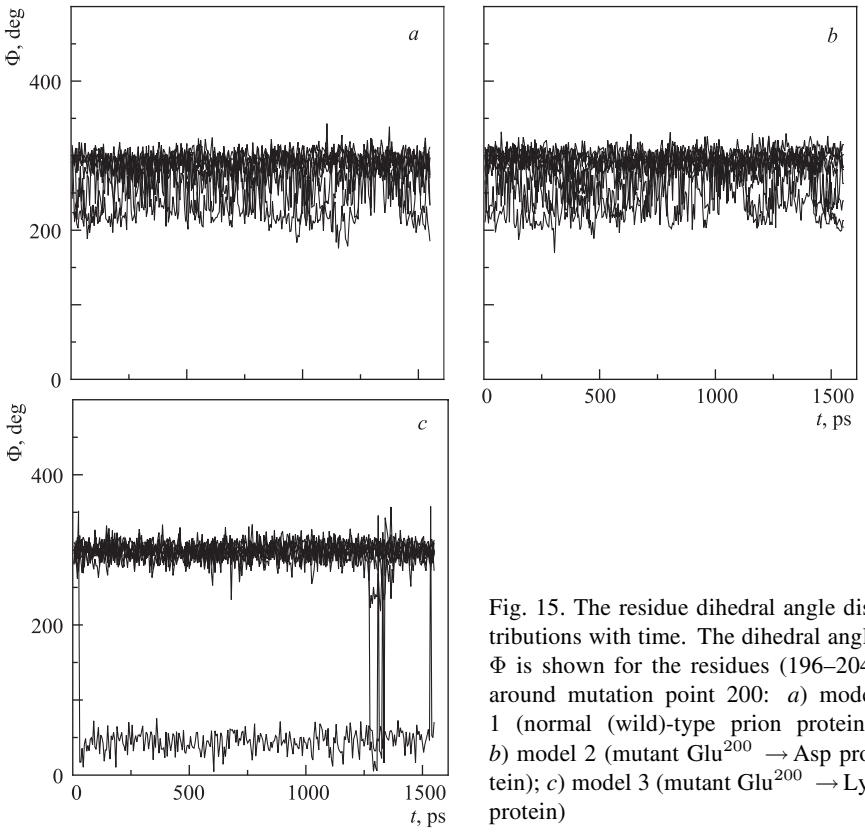

Fig. 15. The residue dihedral angle distributions with time. The dihedral angle Φ is shown for the residues (196–204) around mutation point 200: *a*) model 1 (normal (wild)-type prion protein); *b*) model 2 (mutant $Glu^{200} \rightarrow Asp$ protein); *c*) model 3 (mutant $Glu^{200} \rightarrow Lys$ protein)

As for model 3, in the final structure the atoms of α-helix H1 are positioned very close to the mutation point 200. Thus, a strong contact between the α-helices H1 and H3 causes the H3 to be misfolded in particular and the whole protein structure in total.

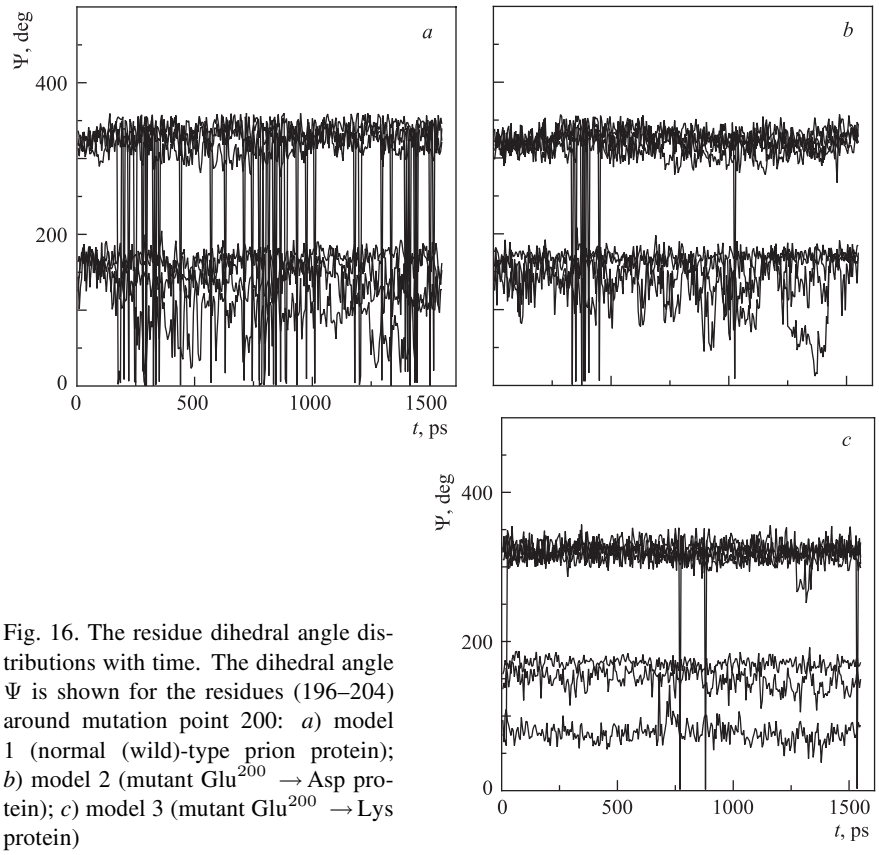

Fig. 16. The residue dihedral angle distributions with time. The dihedral angle Ψ is shown for the residues (196–204) around mutation point 200: *a*) model 1 (normal (wild)-type prion protein); *b*) model 2 (mutant $Glu^{200} \rightarrow$ Asp protein); *c*) model 3 (mutant $Glu^{200} \rightarrow$ Lys protein)

The dihedral angle (Φ and Ψ) distributions for the residues 196–204 around mutation point 200 are presented in Figs. 15 and 16. The snapshots are shown in Figs. 15–16 for all three models under consideration (*a* — model 1; *b* — model 2; *c* — model 3). The Φ and Ψ values of the dynamic simulations and the calculated NMR structures shown in the previous sections seem to be in good agreement. The values of the dihedral angle Φ in the models 1 and 2 are equally distributed (Fig. 15, *a*) and are similar. For the model 3 the Φ distribution jumps around the mutation point (especially on the residue 197) at the beginning of simulations and then it keeps constant till the end (Fig. 15, *c*). Also in model 3 the Ψ values

(Fig. 16) have a distinct behavior, so that this distribution (Fig. 15, *c*) could easily be distinguished from other two models (Fig. 15, *a, b*). These clear differences for the Φ and Ψ distributions suggest the following. As analysis shows, the dihedral angle Φ for the mutant protein is rearranged at residue 197, which belongs to a loop between the α-helices H2 and H3. A rotational transition of Φ (evidently, Ψ) at the mutation point 200 seems to lead to a rearrangement of the nearest residues 196–204 and probably causes formation of a new hydrogen bond network.

6. GENERATION OF A NOVEL HYDROGEN-BOND NETWORK IN THE PRION PROTEIN AS A RESULT OF AMINO-ACID EXCHANGES

A protein structure contains a hydrophobic core, surrounded by a network of hydrogen bonds involving side chains. In this section we present the analysis of the hydrogen-bond network for the initial and final structures of the mutant $Glu^{200} \rightarrow$ Lys prion protein. (The hydrogen bond is regarded to be effective, when the distance between the hydrogen atom of the proton donor and the proton acceptor is less than 2.4 Å.) The results of the previuos section indicate that the prion stuctural rearrangement has to be attributed to a $Glu^{200} \rightarrow$ Lys amino-acid replacement.

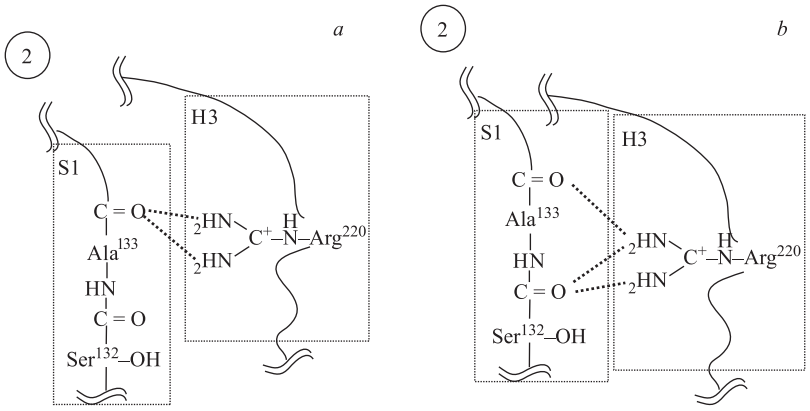

Fig. 17. A schematic diagram of hydrogen-bond network for the initial (*a*) and final (*b*) states in model 3 (mutant $Glu^{200} \rightarrow$ Lys prion protein)

A map of the residue side chains and the hydrogen-bond network are shown in Fig. 17 (*a* — initial state; *b* — final state). At the initial state we have found just

one hydrogen bond around the mutation point Lys^{200}, existing in between Thr^{199}–Asp^{202}, and two hydrogen bonds, which involve Ala^{133} and Arg^{220}. These hydrogen bonds are formed properly. In the final state we can easily see several new hydrogen bonds, which are formed as a result of $Glu^{200} \rightarrow$ Lys substitution (all observed hydrogen bonds in Fig. 17 are displayed along with the residue positions). A new hydrogen bond (shown in Fig. 17, *b*), involves a Ser^{132}–Arg^{220} binding, the side chains of that are exposed to solvent. Two hydrogen bonds involving Ala^{133}–Arg^{220}, which are observed for the initial state, are transformed into a single hydrogen bond. It is known that Glu^{200} is the first residue of the α-helix H3; it is exposed to solvent and does not form any interactions with other parts of the protein. The above results show that the presence of Lys^{200} instead of Glu^{200} changes the protein hydrogen bond of the whole network. In other words, this causes a partially rearranged conformation of the protein structure.

7. SUMMARY

Molecular Dynamics Simulations were performed on rhodopsin and prion proteins to investigate their structural conformation dynamics.

For the rhodopsin (Rh) protein we performed 3-ns simulations and presented the structure analysis results for the Rh dark-adapted state. The root-mean-square deviation (RMSD) data for helices I–VII of Rh were evaluated. From the RMSD data we observed a relative movement of Rh helices, which has not a similar behavior between the helices. Helices I, III, and V exhibit the highest deviations from the reference structure. The stucture images of Rh were constructed from a superposition of the representative configurations at 3-ns state. The results show the largest displacements from the reference structure for helices III and V. The largest deviations are seen in the cytoplasmic region of these helices, the extracellular ends show slight movement. We have also simulated the effect of the E134N mutation on the Rh conformation dynamics. The E134N mutation is considered to be important in the functionality of Rh. This exchange, for example, activates transudin in the absence of the 11-*cis* retinal. We have evaluated the RMSD behavior for the normal Rh and with E134N mutation. The comparison of the analysis data indicates that the reference and E134N mutation structures are subjected to a similar behavior. It is worth noting that nearly each residue in Rh has been examined with site-directed mutagenesis [58, 59, 71]. A selected amino-acid mutation may cause essential changes of the Rh intermolecular interactions mostly due to the electrostatic forces and potentials. There have been several important amino acids (E134N, E122Q, D83N, etc.) to play an essential role in the Rh functions (the protonation mechanism, etc.) [15, 55, 56]. We also presented the calculeted values of the RMSDs for the cutoff and no cutoff approximations. The effect of cutoff and no cutoff

calculations on the Rh helice displacements are compared at 2.0-ns configurations. For a selected Rh helice we observed the largest deviations between these two simulation approaches. The RMSDs for helices III and V of Rh deviate at 200 ps from the start of simulations. This fact indicates that the relative helical movement of Rh seems to be sensitive mostly in the cytoplasmic region.

We have performed MD simulations on three models of the human PrP (about 2 million time step/each structure) to investigate the effect of the specific disease-related point mutations on the conformation dynamics. We observed a partial rearrangement of the prion structure due to a $Glu^{200} \rightarrow Lys$ mutation, and provided a detailed mechanism of this process. The presented data analysis includes the final structure configurations, the dihedral angles, the residue distance distibutions, hydrogen-bond network map and other data. The calculated structure images of the prion proteins at the final state (1.6 ns) indicate that the globular domain of the normal PrP is stably maintained during the whole simulation period. For the mutant protein ($Glu^{200} \rightarrow Lys$) the structure has partly rearranged and we observed a collapse of the third (longest) α-helix H3 at the position of the amino-acid residue 219. The comparison of the structure images for the wild-type and abnormal $Glu^{200} \rightarrow Lys$ prions suggests a mechanism of such reorganization: only when the glutamate-to-lysine substitution occurs at the mutation point 200, the helices H1 and H3 come very close to each other. A flexible motion of H1 to H3 results in the protein rearrangement. At that time, H3 interacts with the strand between H1 and S1 and forms probably a new hydrogen bond. In comparison with the experiments our simulation results (the structural data, formation of new hydrogen-bond network, decay of the salt-bridge interaction, etc.) are partly in good agreement [97, 98]. The partially misfolded structure obtained from our simulations might correlate with the known link between $Glu^{200} \rightarrow Lys$ mutation and the nature of the human prion disease. The associated structural changes observed in the MD-simulational trajectories may provide new insights in the biophysics of the prion protein [99–101].

Acknowledgements. This work was supported by CAL (Computational Astrophysics Laboratory) of RIKEN (The Institute of Physical and Chemical Research), Japan. We acknowledge helpful discussions with Dr. Yoshinori Hirano and Dr. Noriaki Okimoto. We acknowledge computer time provided by CAL RIKEN on the supercomputer Fujitsu VPP and special-purposes MDGRAPE-2 computer for the molecular dynamics simulations. The author is grateful to Prof. Toshikazu Ebisuzaki for the software and facility support during the joint collaboration at CAL RIKEN, where the presented study was completed. The author thanks Prof. Evgenii Krasavin, Dr. Mikhail Altaisky and Academician Mikhail Ostrovsky for fruitful discussions.

Appendix A

THE CORRELATION OF THE CUTOFF AND NO CUTOFF METHODS AND THE Rh STRUCTURAL CHANGES

Figures 18 and 19 present the estimated values of the RMSDs for the cutoff and no cutoff approximations. The effect of cutoff and no cutoff calculations in the Rh helice displacement is compared at 2.0-ns configurations. The RMSDs seem to have close values for several Rh helices. However, for the helices III and V we observe the largest deviations. For helice III the RMSD of the cutoff method has to be two times larger than that of no cutoff simulations. On the other hand, the RMSD of the cutoff method for helice V is comparably two times smaller compared with no cutoff method. The RMSDs for the helices III and V deviate at 200 ps from the start of simulations. This indicates that the Rh helical movement has to be sensitive mostly in the cytoplasmic region. The results of Figs. 17 and 18 also indicate on some cautions for molecular simulation approaches to be concerned for an adequate estimation.

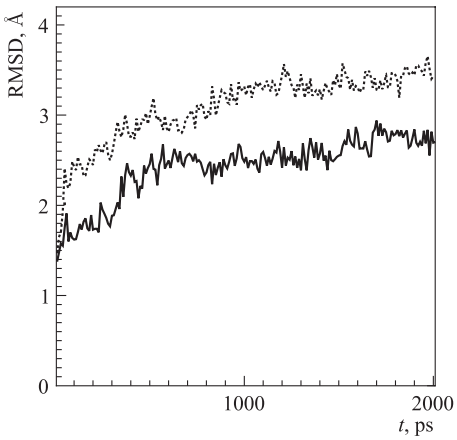

Fig. 18. The RMSD for Rh total structure domain within 2-ns state are shown for cutoff (dotted line) and no cutoff (solid line) MD methods

Appendix B

THE Φ AND Ψ DIHEDRAL ANGLES FOR THE DESCRIPTION OF PROTEINS STRUCTURES

The main chain Φ and Ψ dihedral angles are defined as follows (Fig. 20):

• The Φ angle is the angle of right-handed rotation around N-CA bond, the value being zero if CA-C bond is *cis* to C-N bond.

• The Ψ angle is the angle of right-handed rotation around CA-C bond, the value being zero if C-N bond is *cis* to N-CA bond.

The following procedure can be used to calculate the main chain dihedral angles:

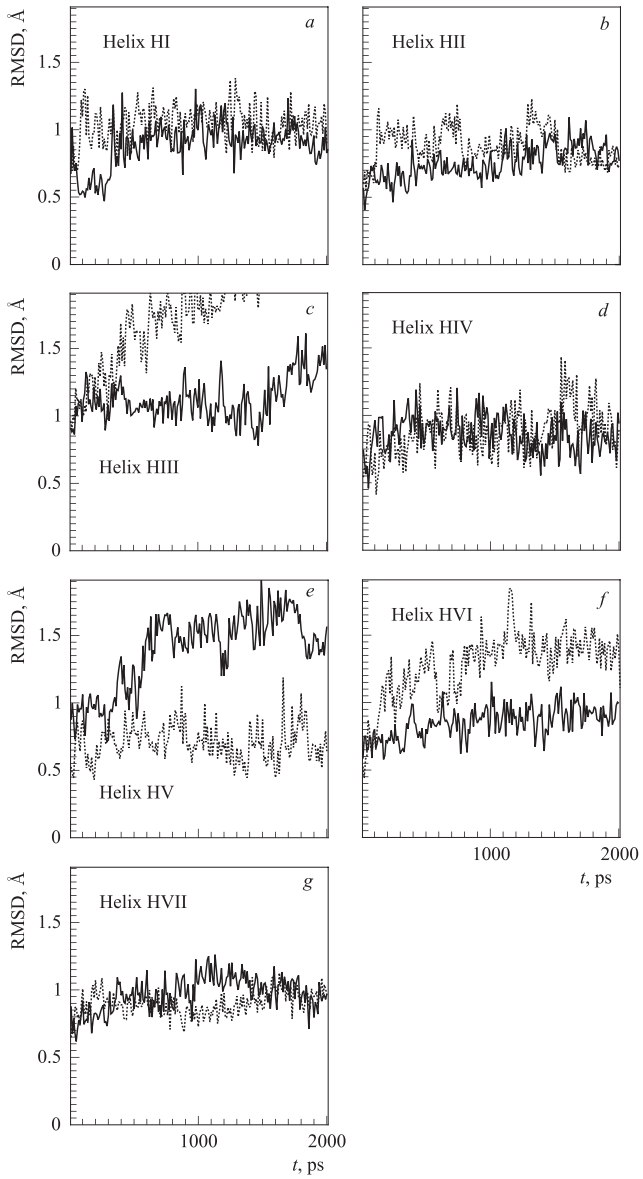

Fig. 19. The RMSDs for helices I–VII of Rh are shown for cutoff (dotted line) and no cutoff (solid line) MD methods

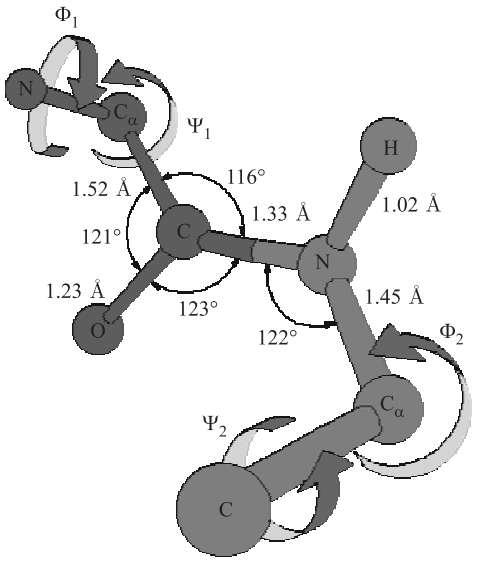

Fig. 20. The Φ and Ψ dihedral angles for the description of proteins structures

1. Firstly, the coordinates of the main chain atoms are used to calculate the dihedral angles Φ and Ψ. The Φ (Ψ) angle will be missing for the first (last) residue in each chain.

2. Secondly, the missing Φ (Ψ) angles will be calculated using the coordinates of H (hydrogen) (O (oxygen)) atoms.

For each side chain dihedral angle, the coordinates of four atoms are required. A detailed description of the proteins dihedral angles is available, for example, from the following homepage:
(http://www.mlb.co.jp/linux/science/garlic/doc/commands/dihedrals.html)

REFERENCES

1. *McCammon J. A., Harvey S. C.* Dynamics of Proteins and Nucleic Acids. Cambridge: Cambridge University Press, 1987.
2. *Allen M. P., Tildesley D. J.* Computer Simulation of Liquids. Oxford: Clarendon Press, 1989.
3. *Warshel A., Parson W. W.* // Q. Rev. Biophys. 2001. V. 34. P. 563–679.
4. *Mazur A. K., Abagyan R. A.* // J. Biol. Struct. Dyn. 1989. V. 6. P. 815–832.
5. *Weiner S. J. et al.* // J. Comp. Chem. 1986. V. 7. P. 230.
6. *Brooks B. R. et al.* // J. Comp. Chem. 1983. V. 4. P. 187–217.
7. *Okada T. et al.* // J. Struct. Biol. 2000. V. 130. P. 73–78.

8. *Shieh T. et al.* // J. Mol. Biol. 1997. V. 269. P. 373–377.
9. *Herzyk P., Hubbard R. E.* // J. Mol. Biol. 1998. V. 281. P. 741–747.
10. *Henderson R., Schertler G. F. X.* // Phys. Trans. Roy. Soc. London. 1990. V. 326. P. 379–389.
11. *Crozier P. S. et al.* // J. Mol. Biol. 2003. V. 333. P. 493–514.
12. *Zrenner E.* // Science. 2002. V. 295. P. 1022–1025.
13. *Palczewski K. et al.* // Science. 2000. V. 289. P. 739–745.
14. *Teller D. C. et al.* // Biochem. 2001. V. 40. P. 7761–7772.
15. *Kandori K., Shichida I., Yoshizawa T.* // Biokhimiya. 2001. V. 66. P. 1483–1498.
16. *Pan D., Mathies R. A.* // Biochem. 2001. V. 40. P. 7929–7936.
17. *Humphrey W. et al.* // Biophys. J. 1998. V. 75. P. 1689–1699.
18. *Tajkhorshid E. et al.* // Biophys. J. 2000. V. 78. P. 683–693.
19. *Hayashi S., Tajkhorshid E., Schulten K.* // Biophys. J. 2002. V. 83. P. 1281–1297.
20. *Saam J. et al.* // Ibid. P. 3097–3112.
21. *Warshel A.* // Nature. 1976. V. 260. P. 679–683.
22. *Birge R. R., Hubbard L. M.* // J. Am. Chem. Soc. 1980. V. 102. P. 2195–2205.
23. *Warshel A., Barboy N.* // Ibid. V. 104. P. 1469–1476.
24. *Tallent J. R. et al.* // J. Am. Chem. Soc. 1992. V. 114. P. 1581–1592.
25. *Rohrig U., Guidoni L., Rotlisberger U.* // Biophys. J. 2002. V. 82. P. 223a.
26. *Choi G. et al.* // Biochem. 2002. V. 41. P. 7318–7324.
27. *Kholmurodov K., Ebisuzaki T.* // ICMS-CSW2004, Tsukuba, 2004. V. C4. P. 9–11.
28. *Kholmurodov K. et al.* // Part. Nucl. 2003. V. 34, No. 2. P. 474–510.
29. *Prusiner S. B.* // Annu. Rev. Microbiol. 1989. V. 43. P. 345–374.
30. *Stahl N. et al.* // Biochem. 1993. V. 32. P. 1991–2002.
31. *Pan K. M. et al.* // Proc. Nat. Acad. Sci. USA. 1993. V. 90. P. 10962–10966.
32. *Safar J. et al.* // Protein Sci. 1993. V. 2. P. 2206–2216.
33. *Prusiner S. B.* // Trends Biochem. Sci. 1996. V. 21. P. 482–487.
34. *Griffith J. S.* // Nature. 1967. V. 215. P. 1043–1044.
35. *Aguzzi A., Weissmann C.* // Nature. 1997. V. 389. P. 795–812.
36. *Kholmurodov K., Okimoto N., Ebisuzaki T.* // The 16th Meeting of MSSJ (Molecular Simulation Soc. of Japan), Niigata, Japan, Dec. 2003.
37. *Kholmurodov K., Okimoto N., Ebisuzaki T.* // RIKEN Rev. 2002. V. 48. P. 16–18.
38. *Kholmurodov K. et al.* // Abstr. of Meetings of the JPS (Jap. Phys. Soc.). 2002. V. 57. P. 293.
39. The 2nd Intern. Workshop «Radiation Safety for Manned Mission to Mars», COSPAR Colloquium, Dubna, Sept. 28 – Oct. 2, 2003.
40. *Molnar F. et al.* // J. Mol. Struct. (Theochem.). 2000. V. 506. P. 169–178.
41. *Ostrovsky M. A. et al.* // Mol. Vision. 2002. V. 8. P. 72–78.
42. *Truchanov K. A. et al.* // Dokl. Akad. Nauk. 2003. V. 377, No. 5. P. 715–717.
43. *Soustov L. V. et al.* // Ibid. V. 388, No. 5. P. 683–688.

44. *Smith W., Forester T. R.* // Comp. Phys. Commun. 1994. V. 79. P. 52–62; see also www.dl.ac.uk/TCS/Software/DL_POLY

45. *Darden T., York D., Pedersen L. G.* // J. Chem. Phys. 1993. V. 98. P. 10089–10092.

46. *Essmann U. et al.* // J. Chem. Phys. 1995. V. 103. P. 8577–8593.

47. *Kholmurodov K. et al.* // J. Comp. Chem. 2000. V. 21. P. 1187–1193.

48. *Kholmurodov K. et al.* // Comp. Phys. Commun. 2000. V. 125. P. 167–182.

49. *Kholmurodov K. et al.* // Proc. High Performance Comp. and Appl., Hokkaido, 2000.

50. *Sakmar T. P., Franke R. R., Khorana H. G.* // Proc. Nat. Acad. Sci. USA. 1989. V. 86. P. 8309–8313.

51. *Birge R. R.* // Biochim. Biophys. Acta. 1990. V. 1016. P. 293–327.

52. *Farrens D. L. et al.* // Science. 1996. V. 274. P. 768–780.

53. *Khorana H. G.* // Proc. Nat. Acad. Sci. USA. 1993. V. 90. P. 1166–1171.

54. *Gelther U., Kobilka B. K.* // J. Biol. Chem. 1998. V. 273. P. 17979–17982.

55. *Kuwata O. et al.* // Biokhimiya. 2001. V. 66. P. 1588–1608.

56. *Sheikh S. P. et al.* // Nature. 1996. V. 383. P. 347–350.

57. *Farahbakhsh Z., Hideg K., Hubbell W.* // Science. 1993. V. 262. P. 1416–1419.

58. *Hubbell W., Cafiso D., Altenbach C.* // Nature Struct. Biol. 2000. V. 7. P. 735–739.

59. *Altenbach C. et al.* // Biochem. 2001. V. 40. P. 15493–15500.

60. MOE (Molecular Operating Environment). http://www.chemcomp.com; used within 2002–2003, by license of CAL RIKEN.

61. *Case D. A. et al.* AMBER 5. University of California, 1997.

62. *Narumi T. et al.* // Mol. Simulation. 1999. V. 21. P. 401–408.

63. *Narumi T. et al.* // Proc. of the 5th Intern. Conf. on Signal Processing, Beijing, 2000. P. 575–582.

64. *Okimoto N. et al.* // Chem.-Bio. Informatics J. 2003. V. 3, No. 1. P. 1–11.

65. *Cornell W. D. et al.* // J. Am. Chem. Soc. 1995. V. 117. P. 5179–5197.

66. *Jorgensen W. L., Chandrasekhar J., Madura J. D.* // J. Chem. Phys. 1983. V. 79. P. 926–935.

67. *Berendsen H. J. C. et al.* // J. Chem. Phys. 1984. V. 81. P. 3684–3690.

68. *Ryckaert J. P., Ciccotti G., Berendsen H. J. C.* // J. Comp. Phys. 1997. V. 23. P. 327–341.

69. *Sayle R. A., Milner-White E. J.* RasMol: Biomolecular Graphics for All // Trends Biochem. Sci. 1995. V. 20. P. 374–376.

70. *Koradi R., Billeter M., Wüthrich K.* MOLMOL: a Program for Display and Analysis of Macromolecular Structure // J. Mol. Graphics. 1996. V. 4. P. 51–55.

71. *Kim J. et al.* // Proc. Nat. Acad. Sci. USA. 1997. V. 94. P. 14273–14278.

72. *Franke R. et al.* // Science. 1990. V. 250. P. 123–125.

73. *Fahmy et al.* // Proc. Nat. Acad. Sci. USA. 1993. V. 90. P. 10206–10210.

74. Keystone Symp. on Molecular Aspects of Transmissible Spongiform Encephalopathies (Prion Diseases), Breckenridge, Colorado, April 2–6, 2003.

75. *Aguzzi A., Heikenwalder M.* // Nature. 2003. V. 423. P. 127–129.

76. *Caughey B., Kocisko D. A.* // Ibid. V. 425. P. 673–674.

77. *Weissmann C. et al.* // Cold Spring Harbor Symp. Quant. Biol. 1996. V. 61. P. 511–522.

78. *Riek R. et al.* // Proc. Nat. Adad. Sci. USA. 1998. V. 95. P. 11667–11672.
79. *Zuegg J., Gready J. A.* // Biochem. 1999. V. 38. P. 13862–13876.
80. *Wills R. G. et al.* // Lancet. 1996. V. 347. P. 921–925.
81. *Riek R. et al.* // Nature. 1996. V. 382. P. 180–182.
82. *James T. L. et al.* // Proc. Nat. Acad. Sci. USA. 1997. V. 94. P. 10086–10091.
83. *Donne D. G. et al.* // Ibid. V. 94 P. 13452–13457.
84. *Riek R. et al.* // FEBS Lett. 1997. V. 413. P. 282–288.
85. *Liu H. et al.* // Biochem. 1999. V. 38. P. 5362–5377.
86. *Zahn R. et al.* // Proc. Nat. Acad. Sci. USA. 2000. V. 97. P. 145–150.
87. *García L. F. et al.* // Ibid. P. 8334–8339.
88. *Shmerling D. et al.* // Cell. 1998. V. 93. P. 203–214.
89. *Liemann S., Glockshuber R.* // Biochem. 1999. V. 38. P. 3258–3267.
90. *Korth C. et al.* // Nature. 1997. V. 390. P. 74–77.
91. *Morrissey M. P., Shakhnovich E. I.* // Proc. Nat. Acad. Sci. USA. 1999. V. 96. P. 11293–11298.
92. *Hanan E. et al.* // Biochem. Biophys. Res. Commun. 2001. V. 280. P. 115–120.
93. *Parchment O. G., Essex J. W.* // Proteins: Struct. Funct. Gen. 2000. V. 38. P. 327–340.
94. *Billeter M., Wüthrich K.* // Archiv of Virol. 2000. V. 16. P. 251–263.
95. *Okimoto N. et al.* // Biophys. J. 2002. V. 82. P. 2746–2757.
96. *Berman H. M. et al.* // The Protein Data Bank. Nucleic Acids Res. 2000. V. 28. P. 235–242.
97. *Swietnicki W. et al.* // J. Biol. Chem. 1998. V. 47. P. 31048–31052.
98. *Zhang Y. et al.* // J. Biol. Chem. 2000. V. 43. P. 33650–33654.
99. *Mead S. et al.* // Science. 2003. V. 300. P. 640–643.
100. *Meier P. et al.* // Cell. 2003. V. 113. P. 49–60.
101. *Kholmurodov K. T. et al.* // Chem.-Bio. Informatics J. 2003. V. 3, No. 2. P. 86–95.